Low-Photon Holographic Phase Retrieval

David A. Barmherzig[1] **and Ju Sun**[2]

[1]*Center for Computational Mathematics, Flatiron Institute, New York, NY 10010, USA*
[2]*Dept. of Computer Science, University of Minnesota, Minneapolis, MN 55455, USA*

[1]*dbarmherzig@flatironinstitute.org,* [2]*jusun@umn.edu*

Abstract: A novel optimization formulation is provided for holographic phase retrieval with data subjected to Poisson shot noise in the low-photon regime. This formulation, based on regularized maximum likelihood estimation, consistently provides improved image reconstruction.

1. Introduction

Holographic phase retrieval (HPR) concerns recovery of a 2D signal (i.e., image) $X \in \mathbb{C}^{n\times n}$ from a set of (pointwise) squared Fourier transform magnitudes

$$Y = \left|\mathscr{F}\left([X, 0_{n\times n}, R]\right)\right|^2 \in \mathbb{C}^{m\times m}, \tag{1}$$

where $\mathscr{F}$ denotes the oversampled Fourier transform operator $\mathbb{C}^{n\times 3n} \to \mathbb{C}^{m\times m}$, and the reference object $R \in \mathbb{C}^{n\times n}$ is known. For simplicity, we can write $\mathscr{F}\left([X, 0_{n\times n}, R]\right) = \mathscr{A}(X) + B$, where $\mathscr{A}(X) = \mathscr{F}\left([X, 0_{n\times 2n}]\right)$ and $B = \mathscr{F}\left([0_{n\times 2n}, R]\right)$.

HPR arises from *holographic coherent diffraction imaging* (HCDI), which is a new scientific imaging technique for resolving nanoscale specimens, such as macroviruses, proteins, and crystals [1]. In HCDI, photon flux intensities are measured using a CCD detector. These values are approximately proportional to the squared magnitudes of the Fourier transform of (the electric field within) a specimen-reference hybrid object, for which the reference is a priori known by experimental design. Thus, recovering the structure of the specimen amounts to solving the HPR problem. The photon flux measurements are often corrupted by *shot noise*—an intrinsic uncertainty due to quantum mechanics, which cannot be removed by any measurement apparatus [1]. Specifically, the measured data are given by

$$\widetilde{Y} \sim \frac{\|Y\|_1}{m^2 N_p} \mathrm{Pois}\left(\frac{m^2 N_p}{\|Y\|_1} Y\right), \tag{2}$$

where $\|Y\|_1 = \sum_{ij}|Y_{ij}|$ is the ℓ_1 norm of Y, $\mathrm{Pois}(\cdot)$ denotes the (pointwise) Poisson distribution, and N_p is a physical constant representing the average number of photons that each pixel of the detector receives. Note that the expectation of $\widetilde{Y}$ is Y, and its variance is inversely proportional to N_p [1].

When N_p is sufficiently large (e.g., $\sim$100 to 1000), the shot noise is less of a concern, and HPR can be solved robustly by linear deconvolution [1, 2] or Wiener filtering [3]. When N_p is small, i.e., in the low-photon regime, however, these established methods perform poorly, as the statistical property of the noise is not taken into account.

2. Regularized Maximum Likelihood Optimization

To account for the Poisson (shot) noise, a natural strategy is given by minimization of the Poisson distribution negative log-likelihood function. For specimens that are of predominant interest in HCDI applications, we also expect the resulting images to be piecewise smooth, similarly to natural images, or with sparsely distributed spatial gradients. This is captured by the popular total variation norm, which we write as $\mathrm{TV}(\cdot)$. Thus, the new formulation we consider in this work is

$$\min_{X\in\mathbb{C}^{n\times n}} F(X) = \sum_{i,j=1}^{m}\left(\left|\mathscr{A}(X)_{ij} + B_{ij}\right|^2 - \widetilde{Y}_{ij}\log\left(\left|\mathscr{A}(X)_{i,j} + B_{i,j}\right|^2\right)\right) + \lambda \mathrm{TV}(X). \tag{3}$$

Here, λ controls the strength of the TV regularization, and

$$\mathrm{TV}(X) = \|\nabla_x X\|_1 + \|\nabla_y X\|_1, \tag{4}$$

where $\nabla_x X \doteq G_x \star X$, $\nabla_y X \doteq G_y \star X$ are directional derivatives and G_x, G_y are the classic *Sobel filters* that implement center-difference derivatives.

Problem (3) is nonsmooth and nonconvex, and the TV term is reminiscent of the alternating direction method of multiplier (ADMM) algorithm that has been successfully deployed in numerous similar problems. However, we find that empirically ADMM struggles to find a feasible solution after we perform variable splitting. Instead, we solve (3) directly using the classic L-BFGS quasi-Newton method. Although L-BFGS is developed for smooth functions, previous studies have demonstrated its successful performance on a variety of practical nonsmooth problems [4].

3. Numerical Simulations

Extensive numerical experiments were conducted using the L-BFGS quasi-Newton method to optimize Problem (3), to be referred to as MLOpt. This performance was compared to the leading HPR methods (namely, inverse filtering and Wiener filtering). Results across a broad range of experimental setups (e.g. various N_p values, reference choices, detector sizes, beamstop sizes, etc.) clearly demonstrate the advantage of MLOpt in the low-photon regime. For example, simulated data values with $N_p = 1$ were generated using the specimen and reference setup shown in Fig. 1. The reconstructed images in Fig. 2 clearly illustrate the advantage of MLOpt in the low-photon regime.

Fig. 1. Specimen (the mimivirus [5]) and reference object (the uniformly redundant array [6]) used in simulation. Both specimen and reference objects are of size 256×256 pixels, and are separated by a 256×256 zero-valued region.

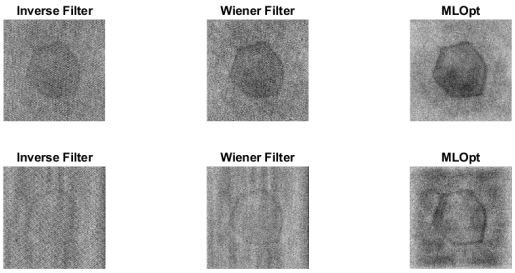

Fig. 2. Algorithm comparison. Simulated data is of size 512×1536 (i.e. two-times oversampling), with an average photon per pixel value of $N_p = 1$. The top row shows the recovered specimen using inverse filtering, Wiener filtering, and MLOpt, respectively, for data with no zeroed-out entries. The bottom row shows the recovered specimen using the same various algorithms, respectively, for data with a beamstop of size 51×51 zeroing-out the low-frequencies (as is typical in HCDI experiments). In both cases, MLOpt provides the best image reconstruction.

References

1. D. A. Barmherzig, J. Sun, T. J. Lane, P-N. Li, and E. J. Candès. Holographic phase retrieval and optimal reference design. *Inverse Problems* 35(9), 2019.
2. D. A. Barmherzig, J. Sun, T. J. Lane, P-N. Li, and E. J. Candès. Dual-reference design for holographic phase retrieval. *2019 International Conference on Sampling Theory and Applications (SampTA)*. 2019.
3. H. He, M. Howells, S. Marchesini, H. N. Chapman, U. Weierstall, H. A. Padmore, J. C. H. Spence. Use of extended and prepared reference objects in experimental Fourier transform X-ray holography. *Applied Physics Letters*. 85(13), 2004.
4. A. S. Lewis and M. L. Overton. Nonsmooth optimization via quasi-Newton methods. *Math. Program.*. 141:13–163, 2012.
5. E. Ghigo et. al. Ameobal Pathogen Mimivirus Infects Macrophages through Phagocytosis. *PLOS Pathogens*. 4(8), 2008.
6. S. Marchesini et. al. Massively parallel X-ray holography. *Nature Photonics*. 2(9), 2008.